RSC Advances

ROYAL SOCIETY
OF CHEMISTRY

www.rsc.org/advances

Unsymmetric Vesicles with a Different Design on Each Side for

Near-Infrared Fluorescence Imaging of Tumor Tissues

Akihiro Uesaka,[a] Isao Hara[b], Tomoya Imai[c], Junji Sugiyama[c] and Shunsaku kimura[*a]

Abstract

Spherical vesicular assemblies with unsymmetric membranes are prepared from the A_3B-type and AB'-type peptides having different helix sense in the hydrophobic B and B' blocks under control of three association factors of stereo-complex formation, dipole-dipole interaction, and steric effect. $[(Sar)_{26}]_3$-b-(L-Leu-Aib)$_6$ (**A₃BL**), $(Sar)_{27}$-b-(L-Leu-Aib)$_6$ (**ABL**), $(Sar)_{28}$-b-(D-Leu-Aib)$_6$ (**ABD**), lipoic-acid terminated **ABL** (**lipoABL**), and lipoic-acid terminated **ABD** (**lipoABD**) are mixed with keeping equi-molar ratio of the total amounts of the right- and the left-handed helices. When **A₃BL** exceeds more than 60% in all the right-handed helices of the mixtures, the unsymmetric vesicles are formed as indicated by selective adsorption of gold nanoparticles to the vesicle surface by TEM observations. The unsymmetric vesicles are also prepared with using **ICGABL** and **ICGABD** having a near-infrared fluorophore, indocyanine green (ICG), at the terminals of **ABL** and **ABD**, respectively. The unsymmetric vesicle formation is verified by fluorescence quenching with the addition of In ions to the solution. When these vesicles are injected into tumor-bearing mice, the vesicles are accumulated into tumor tissues effectively by the EPR effect. The unsymmetric vesicle

having ICG at the inward surface induces the less IgM production than that having ICG at the

outward surface. The more stealth vesicle in the blood stream is therefore obtainable by concealing

the imaging fluorophores in the vesicle.

1. Introduction

Amphiphilic molecules are self-assembled into molecular assemblies in water by various

intermolecular interactions such as hydrophobic and electrostatic interactions.[1–5] Their morphologies

heavily depend on the chemical structure of the components, and suitable molecular designs have

been proposed to generate molecular assemblies with various morphologies and sizes.[6–8] In addition,

molecular assemblies have been applied for broad fields ranging from nanodevices to

biomaterials.[9–14]

Among them, vesicle is one of the most frequently appearing nanocarriers for tumor-targeted drug

delivery and molecular imaging.[15–20] In tumor tissues, the vascular walls have submicron holes

because of the rapid angiogenesis, and therefore nanocarriers can permeate into tumors through the

vascular wall. Furthermore, the lymph system around tumors grows so slowly that nanocarriers are

usually retained in the tumor. This effect is called the enhanced permeability and retention (EPR)

effect.[21] In this regard, the control of the nanocarrier size is essential to allow them to be

accumulated into tumor tissues passively.[18,22,23] Various vesicles of liposomes, polymersomes, and

peptosomes, which were prepared from lipids,[24,25] polymers,[26,27] and peptides,[18,28] respectively, have been studied. One challenge of the vesicular molecular assemblies is to prepare unsymmetric vesicles having different components between the outer and the inner surfaces, which mimic cell membranes. For example, Fuhrhop reported that unsymmetric bolaamphiphiles with a small and a large head groups self-assembled into unsymmetric monolayer vesicles using the steric effect.[29,30] Further, Xiao and Pautot reported that reversed micelles were transferred to a lipid monolayer at the oil/water interface to form unsymmetric vesicles.[31,32] However, it's not so easy to prepare unsymmetric membranes under precise control of the distribution of the components. In addition, these methods seem to be unavailable for amphiphilic polymers to self-assemble in an unsymmetric way due to the disorder packing and/or the molecular entanglement of the hydrophobic blocks.

We previously reported that left-handed helical peptides with one hydrophilic chain (AB-type) and right-handed helical peptides with three hydrophilic chains (A_3B'-type) co-assembled into unsymmetric peptosomes using stereo-complex formation, dipole-dipole interactions, and steric effects.[33] Stereo-complex formation and dipole-dipole interactions can make the helix packing being regularly interdigitated to generate unsymmetric planar sheets. The planar sheets grew into unsymmetric vesicles due to the steric effect of the bulky hydrophilic A_3 moieties of the A_3B-type peptides extruding to the outer surface. Further, the selective surface modification at the outer or the

inner surface can be easily performed by choosing the right-handed or the left-handed helix of the functionalized helical peptides.

In this paper, we study a necessary proportion of the A_3B-type helix, $[(Sar)_{26}]_3$-b-(L-Leu-Aib)$_6$ (**A$_3$BL**), for generation of unsymmetric vesicles in the mixtures of the A_3B-type right-handed helical peptide (**A$_3$BL**), the AB-type right-handed helical peptide, $(Sar)_{27}$-b-(L-Leu-Aib)$_6$ (**ABL**), AB-type left-handed helical peptide, $(Sar)_{28}$-b-(D-Leu-Aib)$_6$ (**ABD**), two AB-type helical peptides with lipoic acid at the terminal of hydrophilic chains, **lipoABL** and **lipoABD** (Fig. 1). Lipoic acid at the terminal of poly(sarcosine) chain has been shown to behave as a hydrophilic group in these molecular assemblies.[33,34] Unsymmetric vesicles about the location of near infrared fluorescent (NIRF) probe are also prepared here by using the novel functional AB-type helical peptides modified with indocyanine green (ICG), **ICGABL** and **ICGABD** (Fig. 1). With these two types of unsymmetric vesicles, one with ICG groups on the outer surface and the other on the inner surface, we examine *in vivo* distributions of these vesicles and the IgM productions in tumor-bearing mice to obtain the information of the surface modification effect on the pharmacokinetics of the vesicles.
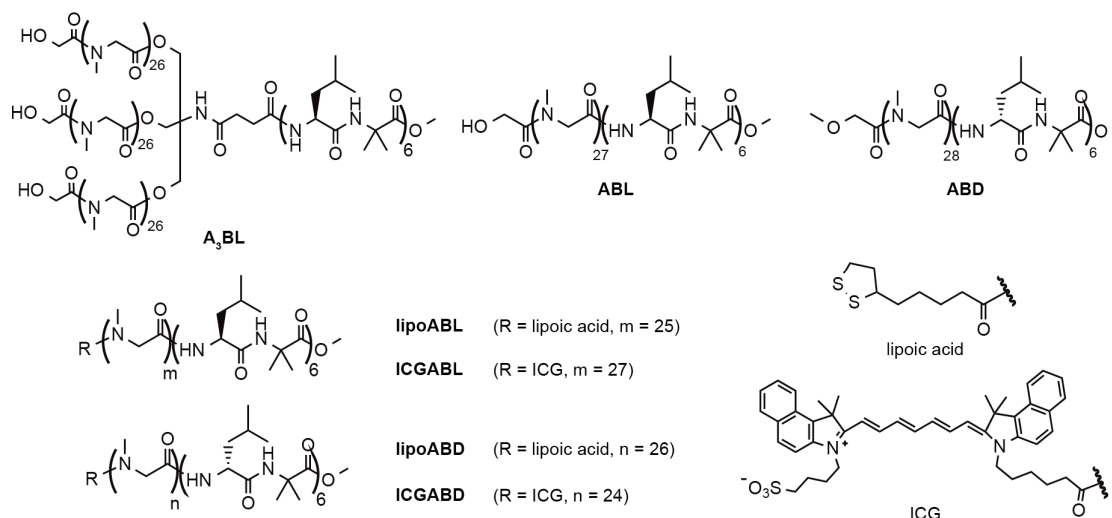
Fig. 1 Chemical structures of amphiphilic block polypeptides **A₃BL**, **ABL**, **ABD**, **lipoABL**,

lipoABD, **ICGABL**, and **ICGABD**.

2. Experimental Section

2.1 Materials

The amphiphilic peptides, **A₃BL**, **ABL**, **ABD**, **lipoABL** and **lipoABD** were obtained as reported

previously.[33,34] **ICGABL** and **ICGABD** were synthesized according to Scheme S1 (ESI†). The

synthetic details are described in the supporting information. Near infrared fluorescence compound,

ICG-sulfo-OSu, was purchased from Dojin Laboratory Ltd. Au nanoparticles (AuNP) were purchased

from BB international (U.K.) with an average diameter of 10 nm. All reagents were purchased

commercially and used as received unless otherwise noted.

2.2 Preparation of Molecular Assembly

The solution of polypeptides in ethanol (0.05 mg/µL, 5.0 µL) was injected into milliQ with stirring

at 4 °C. In the case of **A$_3$BL**, methanol was used instead of ethanol. After 30 min, the dispersion was

heated by aluminum heat source if necessary, followed cooling down at room temperature for

measurements.

2.3 Transmission Electron Microscopy (TEM)

TEM images were taken by using a JEOL JEM-2000EXII at an accelerating voltage of 100 kV.

Peptide aqueous solutions were applied on a carbon-coated Cu grid, and the samples were negatively

stained with 2% uranyl acetate, followed by suction of the excess fluid with a filter paper.

2.4 Frozen-Hydrated/Cryogenic-TEM (Cryo-TEM)

The peptide dispersions were frozen quickly in liquid ethane, which was cooled with liquid nitrogen.

The samples were examined at 100 kV accelerating voltage at the liquid nitrogen temperature.

2.5 Dynamic Light Scattering (DLS)

The DLS measurements were taken using DLS-8000KS (Photal Otsuka Electronics) using He-Ne

laser at 25 °C. Before DLS measurements, each prepared sample was filtered by 0.20 µm PVDF

(polyvinylidene fluoride) syringe filter (GE Healthcare UK limited).

2.6 The Adhesion of AuNPs to Vesicles

Preliminary, peptides with lipoic acid are mixed with the solution of amphiphilic peptides and the

molecular assemblies were prepared from the solutions according to the procedure previously

described.[33] The peptide aqueous solutions were applied on a carbon-coated Cu grid, and then AuNPs

with diameter of 10 nm were added on the grid to reduce non-specific association of AuNPs with

vesicles. Lipoic acids on the molecular assemblies can easily react with AuNPs on the Cu grid.[33,34]

After washing excess amount of AuNPs with dispersion media, the samples were negatively stained

with 2% uranyl acetate, followed by suction of the excess fluid with a filter paper.

2.7 Fluorescent Analysis

The fluorescent spectra of the peptide dispersions were obtained using JASCO FP-6600

spectrofluorometer at an optional temperature with a transmission cell of 1 cm optical path length.

Before measurements, vesicle suspensions were diluted to 0.05 mg/mL (the total volume is 2.0 mL).

The excitation wavelength of ICG is 755 nm.

2.8 *In vivo* NIRF-imaging with vesicles with ICG

The SUIT2/pEF/LUC cells (5×10^5 cells) were dissolved in PBS (20 μL) and subcutaneously

inoculated into the right femoral region of 7-week-old BALB/c nu/nu mice (*n* = 3 per group). Vesicles

containing ICG were prepared in milliQ and NaCl was added into the suspensions to adjust to

physiological condition (0.9 wt% NaCl aq.). The vesicle suspensions (5 mg/kg, 100 µL) were injected

via the tail vein to the mice 1 week after the tumor transplantation. The injected ICG amount was 10

nmol/kg. NIRF images (Ex, 785 nm; Em, 845 nm) were taken at 15 min, 1 h, 3 h, 6 h, 9 h, and 24 h

after the dose. During the imaging process, the mice were held on the imaging stage under

anesthetized condition with 2.5% of isoflurane gas in air flow (1.5 L/min). The pseudo images were

constructed from the photon counts.

2.9 IgM Assay

For ELISA, vesicles (5 mg/kg, 100 µL) were injected to the BALB/c nu/nu mouse, which were

purchased from Japan SLC, Inc. (Japan) ($n = 3$ per group). Mouse blood was collected in 1.5 mL tube

from inferior vena cava under anesthesia condition at 1 week after administration. The serum was kept

overnight at 4 °C. The next day, the serum was obtained by centrifugation (10 min, 3000 rpm) and

saved at -40 °C.

Lactosomes prepared from [poly(Sar)$_{50}$]$_3$-b-poly(L-lactic acid)$_{30}$ in 50 µL acetonitrile was added to

96-well plates (0.5 µg/well) and air dried completely for 1 day. Then, 150 µL blocking buffer [2%

BSA/phosphate-buffered saline (PBS)] was added and incubated for 2 h. The wells were washed four

times with washing buffer (PBS-T: 0.05% tween 20 in PBS). The sera with serial dilution were added

to the wells and incubated for 2 h. After incubation, the wells were washed four times using PBS-T.

Peroxidase-conjugated goat-anti-mouse IgM in 0.1% BSA/PBS (50 μL, Southern Biotech, USA) was

added as the secondary antibody. After incubation of the solution for 2 h, the wells were washed again

four times with PBS-T. *o*-phenylenediamine (0.5 mg/mL, Sigma, St. Louis, MO) dissolved in

0.0003% H_2O_2-0.1 M citrate phosphate buffer (pH 5.0) was added to the well. At 10 min after the

o-phenylenediamine addition, OD was determined at 490 nm with 620 nm as reference.

2.10 Statistical Analysis

All results are expressed as mean ± SD. Differences between groups in AuNP attached on vesicles,

IgM production and NIRF-imaging studies were assessed by the *t*-test for independent samples.

P-value <0.05 and <0.01 are considered statically significant and designated by * and **, respectively.

2.11 Ethics

All of our *in vivo* animal experiments were approved by the animal research committee of Kyoto

University. The animals were treated humanly.

3. Results and Discussions

3.1 Preparation of Unsymmetric Vesicles

A₃BL and **ABD** were co-assembled into planar sheets of *ca*. 150 nm length in milliQ (Fig. 2a), and

these sheets transformed into vesicles of *ca*. 90 nm diameter upon heating at 90 °C for 1 h (Fig. 2b).

DLS measurements show that diameter of the vesicle was 99.6 nm with a narrow size distribution

(PDI = 0.052). These results suggest that the stereo-complex formation contributes to formation of the

planar sheet morphology, and the subsequent heat treatment triggers vesicle formation so as to reduce

the hydrophobic edges in water as reported previously.[33–35]
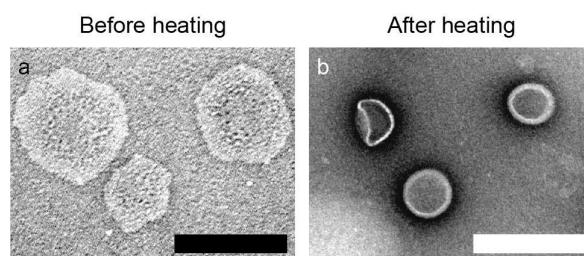
Fig. 2 TEM images (negative stain with 2% uranyl acetate) of molecular assemblies prepared from

A₃BL and **ABD** in milliQ (a) before and (b) after a heat treatment at 90 °C for 1 h. Bars indicate 200

nm.

To study the unsymmetry of the vesicle, **lipoABL** and **lipoABD**, which can bind AuNPs, were

incorporated to the vesicles prepared from **A₃BL** and **ABD**.[33] In the previous paper, we demonstrated

that lipoic acid at the hydrophilic chain terminal behaved as a hydrophilic moiety.[33,34] If lipoic acids of

amphiphilic peptides are oriented to the inside of vesicles, AuNPs shouldn't adhere to vesicles, which

can be visualized by TEM to provide information of the peptide orientation in the membrane. AuNPs

adhered clearly to the vesicles prepared from **A₃BL** + **ABD** + **lipoABL** (0.4/0.5/0.1, mol/mol/mol)

(Fig. 3a and S2a of ESI†), whereas there are few AuNPs on the vesicles prepared from **A₃BL** + **ABD** +

lipoABD (0.5/0.4/0.1, mol/mol/mol) (Fig. 3b and S2b of ESI†). The TEM images show the collapsed

vesicles due to the vacuum condition of the TME observation, but the morphology was confirmed to

be spherical by Cryo-TEM observation (Fig. 5). These results indicate that the unsymmetric vesicles

were formed with the ternary mixtures, and the functionalized peptides with lipoic acid were

integrated in the membrane under control of the molecular orientation according to the right- or

left-handed helical sense of the functionalized peptides.
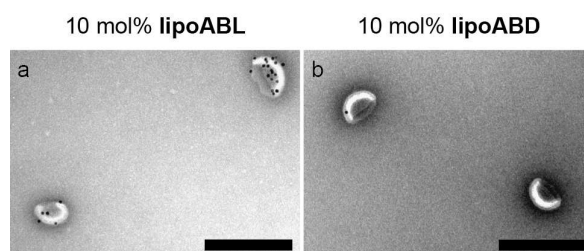
Fig. 3 TEM images (negative stain with 2% uranyl acetate) of vesicles prepared from (a) **A₃BL** +

ABD + **lipoABL** and (b) **A₃BL** + **ABD** + **lipoABD** in milliQ upon a heat treatment at 90 °C for 1 h. An

aliquot of a 10 nm AuNP suspension was added to the vesicles on the TEM grid. Bars indicate 200 nm.

3.2 The effect of A₃BL proportion on unsymmetric membranes

To evaluate the necessary proportion of **A₃BL** in all the right-handed helices to achieve the

unsymmetric vesicles by steric effects, the composition of **ABL** and **A₃BL** was varied (Fig. 4). As

described above, several AuNPs adhered to the vesicles of **A₃BL** + **ABD** + **lipoABL** (0.4/0.5/0.1,

mol/mol/mol), but few AuNPs to the vesicles of **A₃BL** + **ABD** + **lipoABD** (0.5/0.4/0.1, mol/mol/mol).

The latter AuNP adherence was similar extent to that to the vesicles without the lipoic acid-modified

peptides (Fig. S3e of ESI†), suggesting nonspecific adherence of AuNPs in these cases. The

quaternary mixture vesicle of **A₃BL**, **ABL**, **ABD**, and **lipoABL** (0.30/0.10/0.50/0.10, vesicle **c** in Fig.

4), which corresponds to a 60% proportion of the A_3B-type peptide in all the right-handed helices,

clearly attached AuNPs (Fig. S3a of ESI†). On the other hand, when **lipoABL** was replaced by

lipoABD with keeping a 60% proportion of the A_3B-type peptide in all the right-handed helices, the

quaternary mixture vesicle of **A₃BL**, **ABL**, **ABD**, and **lipoABD** (0.30/0.20/0.40/0.10, vesicle **d** in Fig.

4) attached much less AuNPs (Fig. S3b of ESI†). It is therefore indicated that the orientation of the

peptides should be maintained in the unsymmetric way even in the vesicles containing 60% proportion

of the A_3B-type peptide. The numbers of AuNPs adhered to an unit surface area of the vesicles in the

TEM images were counted, and the data are analyzed statistically (Fig. 4). The selective adherence of

AuNPs to the vesicles **a**, **b**, **c**, and **d** was confirmed statistically by a *p*-value of less than 0.01. It is

therefore concluded that all the right-handed helices in these vesicles should orient to outside of the

vesicle.

But, when the proportion of the A_3B-type peptide decreased down to 50% in all the right-handed

helices (vesicles **e** and **f** in Fig. 4), AuNPs adhered to these vesicles similarly with each other (Fig.

S3c,d of ESI†). These results suggest that the molecular direction of helices in the membrane can't be

controlled when the vesicles contain less than 50% A_3B-type peptide in all the right-handed helices.

Composition of vesicles (mol%)					
	A_3BL	ABL	ABD	lipoABL	lipoABD
vesicle **a**	40	0	50	10	0
vesicle **b**	50	0	40	0	10
vesicle **c**	30	10	50	10	0
vesicle **d**	30	20	40	0	10
vesicle **e**	25	15	50	10	0
vesicle **f**	25	25	40	0	10
vesicle **g**	30	20	50	0	0
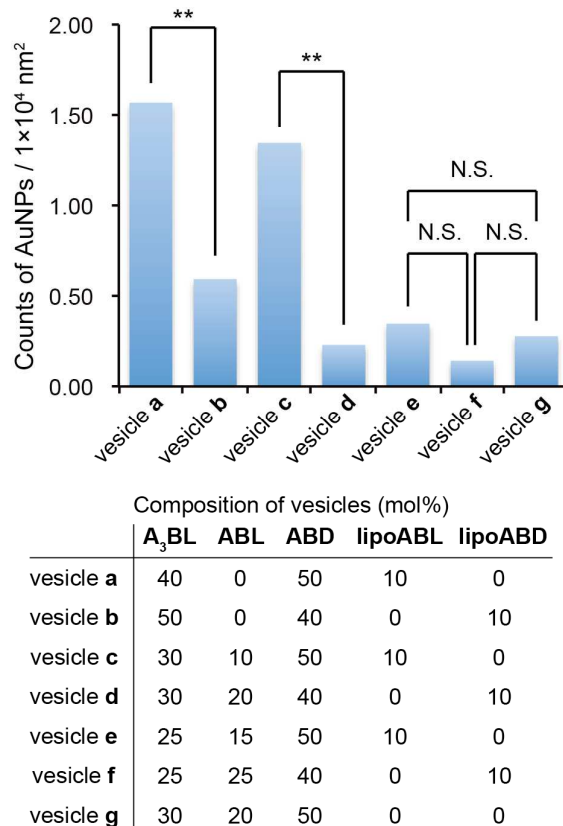
Fig. 4 The number of AuNPs per unit area (100×100 nm^2) of vesicle surfaces. The *p*-value: ** $p <$

0.01.

The DLS measurements revealed that the vesicle diameter became larger by increasing the

proportion of **ABL** in other word by decreasing the proportion of **A₃BL** (Fig. S4 of ESI†). This result

suggests that substituting AB-type peptides for bulky A_3B-type peptides decreases the curvature of

vesicles. Furthermore, the diameter increased sharply when the proportion of **ABL** in all the

right-handed helices is more than 50%. This increase also supports the interpretation that bulky

A_3B-type peptides start to orient to inside of some vesicles when the proportion of **ABL** is more than

50%. From these results, it is considered that unsymmetric vesicles can be prepared in the presence of

A_3BL more than 60% proportion in all the right-handed helices, and the functionalized unsymmetric

vesicles are applicable for some applications which require unsymmetric membranes.

3.3 The Application of unsymmetrical vesicles to NIRF imaging

The unsymmetric vesicles are examined as nanocarriers for NIRF imaging of solid tumor. The

ternary mixtures of **A_3BL** + **ABD** + **ICGABL** (0.48/0.5/0.02, mol/mol/mol) and **A_3BL** + **ABD** +

ICGABD (0.5/0.48/0.02, mol/mol/mol) were self-assembled into homogeneous vesicles in milliQ

(Fig. 5 and S5 of ESI†). These vesicle diameters were 111.7 nm and 111.5 nm by DLS measurements,

which correspond to those of the unsymmetric vesicles described before. Cryo-TEM images confirm

formation of vesicles even in the presence of ICG-peptides in these compositions (Fig. 5).
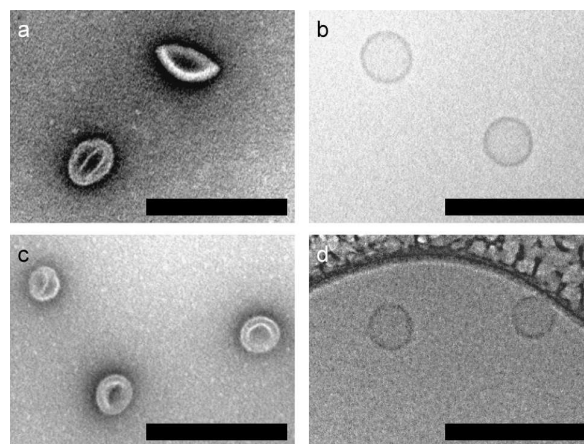
Fig. 5 TEM images (negative stain with 2% uranyl acetate) of vesicles prepared from (a) **A₃BL** +

ABD + **ICGABL** and (c) **A₃BL** + **ABD** + **ICGABD** in milliQ upon a heat treatment at 90 °C for 1 h.

Cryo-TEM images of vesicles prepared from (b) **A₃BL** + **ABD** + **ICGABL** and (d) **A₃BL** + **ABD** +

ICGABD. Bars indicate 200 nm.

To confirm that vesicles containing ICG also have unsymmetric membranes, $InCl_3$ aq. was added to

the vesicle suspension. $InCl_3$ was used as the quencher because hydrophilic poly(sarcosine) chains of

vesicles were suggested to adsorb In^{3+} ions to quench ICG fluorescence effectively by the heavy-atom

effect. When 10 µM $InCl_3$ aq. was added to vesicles containing ICG-peptides, In^{3+} ions quenched

fluorescence more effectively from the vesicle containing **ICGABL** than that containing **ICGABD** by

the Stern-Volmer plots (Fig. 6). The molecular orientation of **ICGABL** and **ICGABD** in each vesicle

is therefore controlled to locate at outside and inside of the vesicles, respectively. In these ternary

mixtures, the **A₃BL** proportions in all the right-handed helix peptides exceed over 96%, and the

unsymmetric vesicle formation with these ternary mixtures is consistent with our interpretation about

the relationship between unsymmetry and composition.
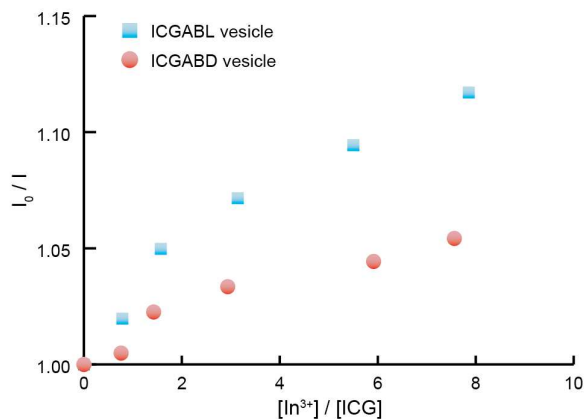
Fig. 6 Stern-Volmer plots of the fluorescence quenching of vesicles containing **ICGABL** (blue

squares) and **ICGABD** (red circles) by In^{3+} ions.

In vivo dispositions of vesicles containing **ICGABL** and **ICGABD** in tumor-bearing mice were

analyzed by NIRF imaging (Fig. 7 and S6 of ESI†). These vesicles were prepared in milliQ and the

concentration of NaCl was adjusted to physiological condition (0.9 wt%) with addition of NaCl. The

hydrodynamic diameters of the vesicle before and after the salt addition were the same to be 112.8 nm

(PDI of 0.080) and 109.0 nm (PDI of 0.083), respectively. Integrity of the vesicle with the addition of

NaCl was also confirmed by Cryo-TEM measurement of the unsymmetric vesicle prepared from

A₃BL + **ABD**. Further, the membrane held the impermeable property against FITC-dextran

incorporated in the vesicle upon the change of ion strength.[33]

The accumulated amounts of the vesicles in tumor at the right femoral region and in the healthy part

of the left femoral region were estimated by the fluorescence intensity of the images. Fig. 7 shows that

the vesicle containing **ICGABD** was accumulated in tumor more than the vesicle containing

ICGABL. Further, the NIRF images at 5 min after the injection show that the vesicle containing

ICGABD spread over the whole body to fluoresce more intensively than the vesicle containing

ICGABL (Fig. 7b). The vesicle concentration in the blood stream at 5 min after the injection should

be therefore higher with the vesicle containing **ICGABD** than that containing **ICGABL**. At the

moment, the clearance time of the vesicle could not be obtained due to the significant capture by liver,

but these observations support that the vesicle containing **ICGABD** should remain in the blood stream

more than the vesicle containing **ICGABL**, which induced the accumulation of the former vesicle in

tumor more that the latter. In the case of the vesicle containing **ICGABD**, the fluorophores were

concealed in the unsymmetric vesicle, which should diminish the capture by liver especially due to the

ICG fluorophore.
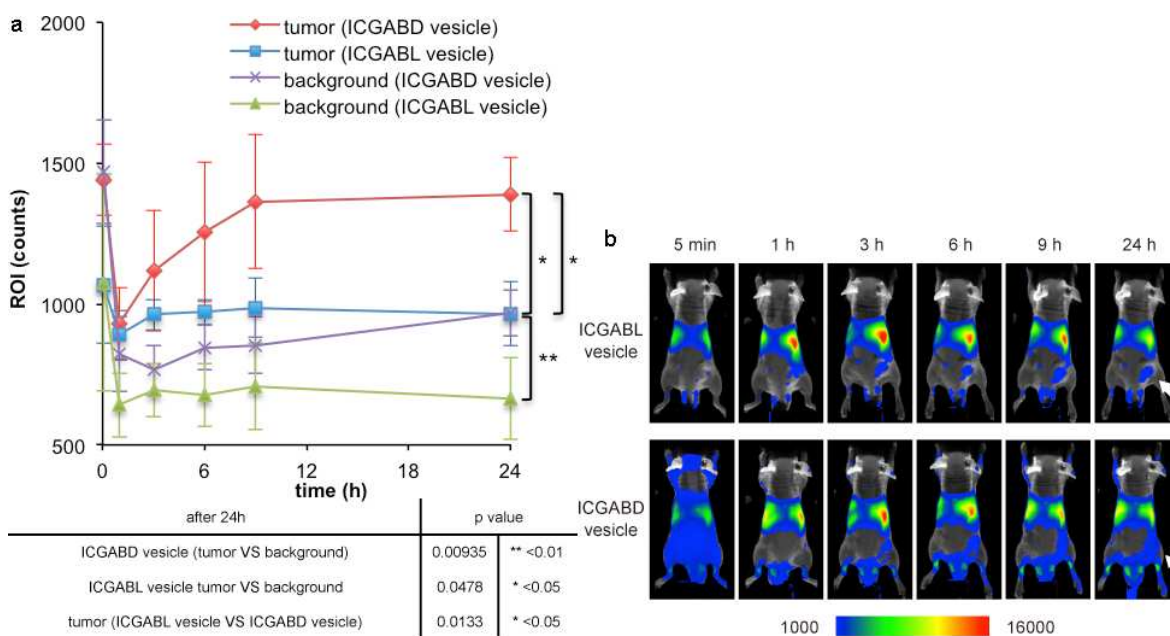
Fig. 7 Accumulations of the vesicles containing **ICGABL** and **ICGABD** in tumor-bearing mice by

NIRF imagings (n = 3). NIRF images were taken at 15 min, 1 h, 3 h, 6 h, 9 h and 24 h after

administration. (a) The vertical axis represents ROI at tumor and background. The p-value: * $p < 0.05$,

** $p < 0.01$ (time point is 24 h). (b) *In vivo* NIRF images were taken at 24 h after administration. For

the NIRF imaging, Clairvivo OPT system was used.

Some nanoparticles have been reported to trigger IgM production when they were dosed to

mice.[36-38] For example, polymeric micelle prepared from poly(Sar)$_{64}$-b-poly(L-lactic acid)$_{30}$ induced

the production of the anti-poly(sarcosine) IgM and IgG with a long memory. The amounts of

anti-poly(sarcosine) IgM produced by the current vesicles were analyzed by ELISA with taking

Lactosome as the positive control (Fig. 8). The vesicles containing ICG-peptides triggered the

production of IgM but with less amounts compared with Lactosome. Ishida *et al.* pointed out that the

surface density influenced the amount of IgM production.[38] On the other hand, we have reported that

the high surface density of poly(sarcosine) chains of nanoparticles suppressed the IgM production.[39]

In the present case, the A_3B-type peptide extruded the bulky A_3 moieties outside, and helical blocks

were packed tightly due to stereo-complex formation. The surface density of poly(sarcosine) should

be therefore higher with the current vesicles than Lactosome. This higher surface density might be the

reason for the current vesicles to suppress the IgM production even though the vesicles have larger

diameter of about 100 nm than Lactosome of 35 nm diameter.

The vesicle containing **ICGABL** triggered the IgM production more than the vesicle containing

ICGABL. Since ICG moieties of the vesicle containing **ICGABL** are exposed to outside of the

vesicle, the surface may have more defects than the vesicle containing **ICGABD** to allow recognition

by B cells easier. It is considered that the unsymmetric vesicles also have different stimulation

property to the immune system.
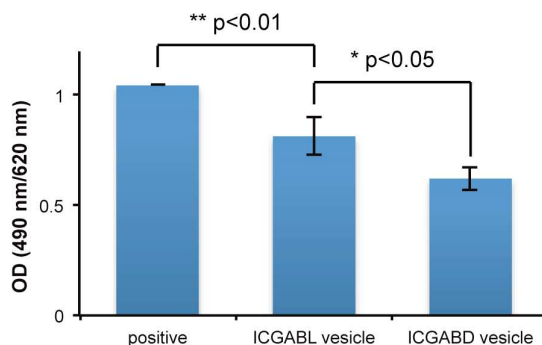
Fig. 8 The production of anti-poly(sarcosine) IgM evaluated by ELISA with using the Lactosome plate. The serum was taken at 7 days after dose of Lactosome (positive), the vesicle containing **ICGABL** (ICGABL vesicle), or the vesicle containing **ICGABD** (ICGABD vesicle). The *p*-value: * *p* < 0.05, ** *p* < 0.01.

Conclusions

Unsymmetric vesicles were prepared from the mixture of A_3B-type right-handed helices and AB-type left-handed helices in milliQ utilizing stereo-complex formation, dipole-dipole interaction and steric effect. More than 60% A_3B-type peptides in all the right-handed helices are necessary to obtain the unsymmetric vesicles as a result of the steric effect. In other words, the vesicles can contain possibly up to 40% functionalized AB-type right-handed helix peptide in all the right-handed helices where all the functional groups are exposed to outside of the vesicle. Further, the functional groups can be concealed in the inner surface of the vesicle with using a functionalized AB-type left-handed helix peptide. As shown in the present paper, the vesicles show different behaviors about the *in vivo* disposition and the reaction with the immune system depending on the location of the function groups on the vesicle. We are currently trying to raise the accumulation amount of the vesicle in tumor and to develop a bimodal imaging vesicle with the unsymmetric vesicle.

Notes and references

[a]*Department of Material Chemistry, Graduate School of Engineering, Kyoto University,*

Kyoto-Daigaku-Katsura, Nishikyo-ku, Kyoto, 615-8510, Japan.

[b]*Technology Research Laboratory, Shimadzu Corporation, 3-9-4 Hikari-dai, Seika-cho, Soraku-gun,*

Kyoto 619-0237, Japan

[c]*Research Institute for Sustainable Humanosphere (RISH), Kyoto University, Gokasho, Uji, Kyoto*

611-0011, Japan.

Corresponding author. E-mail: shun@scl.kyoto-u.ac.jp; Fax: (+81)75-383-2401; Tel:

(+81)75-383-2400

† Electronic Supplementary Information (ESI) available: [details of any supplementary information

available should be included here]. See DOI: 10.1039/b000000x/

1   Bangham, A. D.; Horne, R. W. *J. Mol. Biol.* 1964, **8**, 660–668.

2   Discher, B. M.; Won, Y.-Y.; Ege, D. S.; Lee, J. C.-M.; Bates, F. S.; Discher, D. E.; Hammer, D. A. *Science* 1999, **284**, 1143–1146.

3   Discher, D. E.; Eisenberg, A. *Science* 2002, **297**, 967–973.

4   Koga, T.; Taguchi, K.; Kobuke, Y.; Kinoshita, T.; Higuchi, M. *Chem. – Eur. J.* 2003, **9**, 1146–1156.

5   Liu, Z.; Qiao, J.; Tian, Y.; Wu, M.; Niu, Z.; Huang, Y. *Langmuir* 2014, **30**, 8938–8944.

6   Israelachvili, J. N.; Mitchell, D. J.; Ninham, B. W. *J. Chem. Soc. Faraday Trans. 2 Mol. Chem. Phys.* 1976, **72**, 1525–1568.

7   Hest, J. C. M. van; Delnoye, D. a. P.; Baars, M. W. P. L.; Genderen, M. H. P. van; Meijer, E. W. *Science* 1995, **268**, 1592–1595.

8   Ge, Z.; Liu, S. *Macromol. Rapid Commun.* 2009, **30**, 1523–1532.

9   Braun, E.; Eichen, Y.; Sivan, U.; Ben-Yoseph, G. *Nature* 1998, **391**, 775–778.

10   Scheibel, T.; Parthasarathy, R.; Sawicki, G.; Lin, X.-M.; Jaeger, H.; Lindquist, S. L. *Proc. Natl. Acad. Sci.* 2003, **100**, 4527–4532.

11   Broz, P.; Driamov, S.; Ziegler, J.; Ben-Haim, N.; Marsch, S.; Meier, W.; Hunziker, P. *Nano Lett.* 2006, **6**, 2349–2353.

12 Blanazs, A.; Armes, S. P.; Ryan, A. J. *Macromol. Rapid Commun.* 2009, **30**, 267–277.

13 Dehsorkhi, A.; Castelletto, V.; Hamley, I. W.; Seitsonen, J.; Ruokolainen, J. *Langmuir* 2013, **29**, 14246–14253.

14 Loh, X. J.; Barrio, J. del; Lee, T.-C.; Scherman, O. A. *Chem. Commun.* 2014, **50**, 3033–3035.

15 Ghoroghchian, P. P.; Frail, P. R.; Susumu, K.; Blessington, D.; Brannan, A. K.; Bates, F. S.; Chance, B.; Hammer, D. A.; Therien, M. J. *Proc. Natl. Acad. Sci. U. S. A.* 2005, **102**, 2922–2927.

16 Weissleder, R. *Science* 2006, **312**, 1168–1171.

17 Cho, K.; Wang, X.; Nie, S.; Chen, Z. (Georgia); Shin, D. M. *Clin. Cancer Res.* 2008, **14**, 1310–1316.

18 Tanisaka, H.; Kizaka-Kondoh, S.; Makino, A.; Tanaka, S.; Hiraoka, M.; Kimura, S. *Bioconjug. Chem.* 2008, **19**, 109–117.

19 Liu, Q.; Zhu, H.; Qin, J.; Dong, H.; Du, J. *Biomacromolecules* 2014, **15**, 1586–1592.

20 Ye, F.; Barrefelt, Å.; Asem, H.; Abedi-Valugerdi, M.; El-Serafi, I.; Saghafian, M.; Abu-Salah, K.; Alrokayan, S.; Muhammed, M.; Hassan, M. *Biomaterials* 2014, **35**, 3885–3894.

21 Matsumura, Y.; Maeda, H. *Cancer Res.* **1986**, *46*, 6387–6392.

22 Makino, A.; Kizaka-Kondoh, S.; Yamahara, R.; Hara, I.; Kanzaki, T.; Ozeki, E.; Hiraoka,

M.; Kimura, S. *Biomaterials* 2009, **30**, 5156–5160.

23 Cabral, H.; Matsumoto, Y.; Mizuno, K.; Chen, Q.; Murakami, M.; Kimura, M.; Terada, Y.;

Kano, M. R.; Miyazono, K.; Uesaka, M.; Nishiyama, N.; Kataoka, K. *Nat. Nanotechnol.*

2011, *6*, 815–823.

24 Maruyama, K. *Adv. Drug Deliv. Rev.* 2011, **63**, 161–169.

25 Kraft, J. C.; Freeling, J. P.; Wang, Z.; Ho, R. J. Y. *J. Pharm. Sci.* 2014, **103**, 29–52.

26 Jun, Y. J.; Park, M. K.; Jadhav, V. B.; Song, J. H.; Chae, S. W.; Lee, H. J.; Park, K. S.;

Jeong, B.; Choy, J. H.; Sohn, Y. S. *J. Controlled Release* 2010, **142**, 132–137.

27 Lai, M.-H.; Lee, S.; Smith, C. E.; Kim, K.; Kong, H. *ACS Appl. Mater. Interfaces* 2014, **6**,

10821–10829.

28 Kokuryo, D.; Anraku, Y.; Kishimura, A.; Tanaka, S.; Kano, M. R.; Kershaw, J.; Nishiyama,

N.; Saga, T.; Aoki, I.; Kataoka, K. *J. Controlled Release* 2013, **169**, 220–227.

29 Fuhrhop, J.-H.; Mathieu, J. *J. Chem. Soc. Chem. Commun.* 1983, 144–145.

30 Fuhrhop, J. H.; Fritsch, D. *Acc. Chem. Res.* 1986, **19**, 130–137.

31 Xiao, Z.; Xu, M.; Li, M.; Lu, Z.; Wei, Y. *Supramol. Sci.* 1998, **5**, 619–622.

32 Pautot, S.; Frisken, B. J.; Weitz, D. A. *Proc. Natl. Acad. Sci.* 2003, **100**, 10718–10721.

33 Uesaka, A.; Ueda, M.; Imai, T.; Sugiyama, J.; Kimura, S. *Langmuir* 2014, **30**, 4273–4279.

34 Ueda, M.; Makino, A.; Imai, T.; Sugiyama, J.; Kimura, S. *Soft Matter* 2011, **7**, 4143–4146.

35 Ueda, M.; Makino, A.; Imai, T.; Sugiyama, J.; Kimura, S. *Chem. Commun.* 2011, **47**, 3204–3206.

36 Hara, E.; Makino, A.; Kurihara, K.; Yamamoto, F.; Ozeki, E.; Kimura, S. *Int. Immunopharmacol.* 2012, **14**, 261–266.

37 Hara, E.; Makino, A.; Kurihara, K.; Sugai, M.; Shimizu, A.; Hara, I.; Ozeki, E.; Kimura, S. *Biochim. Biophys. Acta BBA - Gen. Subj.* 2013, **1830**, 4046–4052.

38 Ishida, T.; Harada, M.; Wang, X. Y.; Ichihara, M.; Irimura, K.; Kiwada, H. *J. Controlled Release* 2005, **105**, 305–317.

39 Hara, E.; Ueda, M.; Kim, C. J.; Makino, A.; Hara, I.; Ozeki, E.; Kimura, S. *J. Pept. Sci.* 2014, **20**, 570–577.